Journal of Medicinal Chemistry

Article

Discovery of Selective Small Molecule Inhibitors of Monoacylglycerol Acyltransferase 3 (MGAT3)

Kim Huard, Allyn Timothy Londregan, Gregory Tesz, Kevin B Bahnck, Thomas V Magee, David Hepworth, Jana Polivkova, Steven Coffey, Brandon A. Pabst, James R. Gosset, Anu Nigam, Kou Kou, Hao Sun, Kyuha Lee, Michael Herr, Markus Boehm, Philip A Carpino, Bryan Goodwin, Christian Perreault, Qifang Li, Csilla C. Jorgensen, George Tkalcevic, Timothy A. Subashi, and Kay Ahn

J. Med. Chem., **Just Accepted Manuscript** • DOI: 10.1021/acs.jmedchem.5b01008 • Publication Date (Web): 10 Aug 2015

Just Accepted

ACS Publications

Journal of Medicinal Chemistry is published by the American Chemical Society. 1155 Sixteenth Street N.W., Washington, DC 20036

Discovery of Selective Small Molecule Inhibitors of Monoacylglycerol Acyltransferase 3 (MGAT3)

Kim Huard,[†]* Allyn T. Londregan,[‡]* Gregory Tesz,[#] Kevin B. Bahnck,[‡] Thomas V. Magee,[†] David Hepworth,[†] Jana Polivkova,[‡] Steven B. Coffey,[‡] Brandon A. Pabst,[#] James R. Gosset, [§] Anu Nigam,[#] Kou Kou,[#] Hao Sun,[∇] Kyuha Lee,[#] Michael Herr,[‡] Markus Boehm,[†] Philip A. Carpino,[†] Bryan Goodwin,[#] Christian Perreault,[‡] Qifang Li,[‡] Csilla C. Jorgensen,[∇] George T. Tkalcevic,[∇] Timothy A. Subashi,[∇] Kay Ahn[#]

[†]Worldwide Medicinal Chemistry, [#]Cardiovascular, Metabolic and Endocrine Diseases Research Unit, and [§]Pharmacokinetics, Dynamics and Metabolism, Pfizer Worldwide Research & Development, Cambridge, Massachusetts 02139, United States

[‡]Worldwide Medicinal Chemistry, [∇]Pharmacokinetics, Dynamics and Metabolism, Pfizer Worldwide Research & Development, Groton, Connecticut 06340, United States.

ABSTRACT: Inhibition of triacylglycerol (TAG) biosynthetic enzymes has been suggested as a promising strategy to treat insulin resistance, diabetes, dyslipidemia, and hepatic steatosis.

Monoacylglycerol acyltransferase 3 (MGAT3) is an integral membrane enzyme that catalyzes the acylation of both monoacylglycerol (MAG) and diacylglycerol (DAG) to generate DAG and TAG, respectively. Herein, we report the discovery and characterization of the first selective small molecule inhibitors of MGAT3. Isoindoline-5-sulfonamide (**6f**, PF-06471553) selectively inhibits MGAT3 with high *in vitro* potency and cell efficacy. Because the gene encoding MGAT3 (*MOGAT3*) is found only in higher mammals and humans, but not in rodents, a transgenic mouse model expressing the complete human *MOGAT3* was used to characterize the effects of **6f** *in vivo*. In the presence of a combination of diacylglycerol acyltransferases 1 and 2 (DGAT1 and DGAT2) inhibitors, an oral administration of **6f** exhibited inhibition of the incorporation of deuterium labeled glycerol into TAG in this mouse model. The availability of a potent and selective chemical tool and a humanized mouse model described in this report should facilitate further dissection of the physiological function of MGAT3 and its role in lipid homeostasis.

GRAPHICAL ABSTRACT:

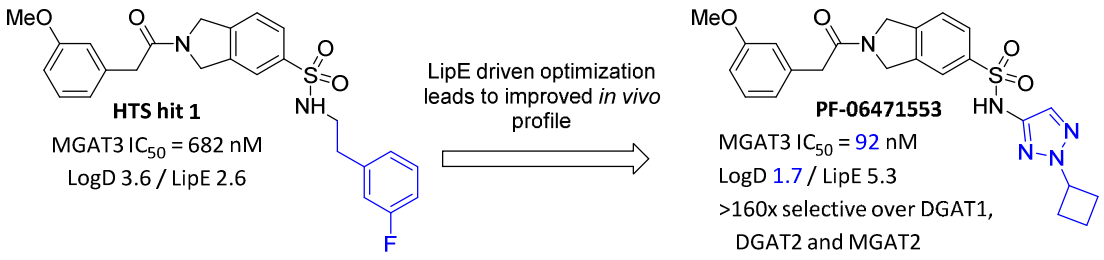

INTRODUCTION

Triacylglycerol (TAG) synthesis serves a critical physiological function for energy storage. However, excessive deposition of TAG and other lipid intermediates in non-adipose tissues is proposed to give rise to a variety of pathological conditions including type 2 diabetes mellitus (T2DM) and nonalcoholic steatohepatitis (NASH).[1] Therefore, inhibition of TAG biosynthetic enzymes has been suggested as a strategy for the treatment of these disorders.

TAG are synthesized by two major pathways, the glycerol-3-phosphate pathway and the monoacylglycerol (MAG) pathway. The glycerol-3-phosphate pathway is present in most cells. In contrast, the MAG pathway is found in specific cell types, such as enterocytes, hepatocytes, and adipocytes. In the MAG pathway, MAG is acylated to yield diacylglycerol (DAG) by monoacylglycerol acyltransferases (MGATs). In the final reaction of both pathways, DAG is further acylated to generate TAG by diacylglycerol acyltransferases (DGATs).[2]

The complexity of TAG synthesis is reflected by the presence of multiple isoforms of MGAT and DGAT enzymes that differ in their catalytic properties, subcellular localization, tissue distribution, and physiological functions. For example, the acylation of DAG to form TAG is catalyzed by two structurally distinct enzymes, DGAT1 and DGAT2, which belong to two distinct gene products.[3] There are three isoforms of MGAT enzymes, known as MGAT1, MGAT2, and MGAT3, which are encoded by three genes, *MOGAT1*, *MOGAT2*, and *MOGAT3*, respectively. They differ in tissue expression patterns and in catalytic properties.[4] The *MOGAT3* gene is found only in humans and higher mammals, but not in rodents.

DGAT1 and its inhibitors are by far the most advanced area of research among these TAG/DAG synthesizing enzymes. DGAT1 inhibitors from multiple pharmaceutical companies were

advanced to the clinic for the potential treatment of an array of metabolic disorders as well as for hepatitis C virus.[5] Pre-clinically, beneficial metabolic phenotypes of DGAT2 inhibition have been demonstrated by antisense oligonucleotide studies[6] and more recently with small molecule inhibitors.[7] It was also shown that MGAT2-deficient mice are protected against diet-induced obesity, glucose intolerance and fatty liver[8] and MGAT2 inhibitors have been reported in the literature.[9]

Although named after its initial enzyme activity, MGAT3 shares higher sequence homology with DGAT2 than the other MGAT isoforms. Human MGAT3 bears 49, 44, and 46% amino acid identity to human DGAT2, human MGAT1, and human MGAT2, respectively.[4e] In addition, MGAT3 demonstrates significantly higher DGAT activity than MGAT1 and MGAT2 when either MAG or DAG is used as substrate, suggesting that MGAT3 also functions as a TAG synthase.[10] Crystallographic structure or studies demonstrating critical active site residues in MGAT3 are still lacking. However, a sequence "HPHG" in MGAT3 is completely conserved in DGAT2, MGAT1, and MGAT2, suggesting that this sequence plays a crucial role in the function of these enzymes. Considering that the site-directed mutagenesis studies on this sequence in DGAT2 showed that the H161A, P162G, and H163A mutants exhibit significantly reduced DGAT2 activity compared to that of the wild type,[11] similar critical roles of these residues are expected for MGAT1-3 functional activity.

We recently reported that hepatic expression of the *MOGAT3* gene highly correlated with MGAT activity measured in liver biopsies from obese human subjects, whereas the *MOGAT1* and *MOGAT2* gene expression did not. Marked weight loss following gastric bypass surgery was shown to be associated with a significant reduction in the *MOGAT2* and *MOGAT3* gene expression, which were also up-regulated in human subjects with nonalcoholic fatty liver disease

(NAFLD).[12] Based on these findings, we sought to explore MGAT3 as a potential target for pharmacological intervention for the treatment of obesity-related insulin resistance and NAFLD.

This report describes the medicinal chemistry efforts associated with the discovery and characterization of the first selective, small-molecule inhibitors of MGAT3 which displayed *in vivo* inhibition of MGAT3. Improvements in lipophilic efficiency (LipE)[13] as well as *in vitro* pharmacokinetic (PK) profile served as general measures of progress.

RESULTS AND DISCUSSION

Measurement of Human MGAT3 Inhibition and *In Vitro* Screening Strategy. MGAT3 possesses both MGAT and DGAT activity.[4e, 10, 12] In order to effectively evaluate and quantify MGAT3 inhibition *in vitro*, we developed an assay which measures its DGAT activity utilizing 1,2-didecanoyl-*sn*-glycerol and [1-^{14}C]decanoyl-CoA as the acyl acceptor and donor, respectively. Under these conditions, the only radioactive product generated was TAG, which simplified the analysis. In contrast, two radioactive products (both DAG and TAG) were generated when measuring MGAT activity of MGAT3 utilizing MAG as the acyl acceptor (data not shown). Human MGAT3 is most closely related to human DGAT2, and therefore, we chose to screen all compounds in parallel against both enzymes. This allowed a rapid selection of compounds with high selectivity. Key compounds were further assessed against a panel of other related acyltransferases including DGAT1, MGAT1, and MGAT2. *In vitro* MGAT1-3 and DGAT1-2 inhibition was assessed as previously described by Futatsugi *et al*.[7]

Hit Identification and Profile. High-throughput screening (HTS) of a subset of the Pfizer compound collection led to the identification of isoindoline-5-sulfonamide **1**, as an inhibitor of MGAT3 (IC_{50} = 682 nM) with excellent selectivity over MGAT1-2 and DGAT1-2 (Figure 1).

Inhibition of MGAT3 activity by **1** was fully reversible in rapid dilution experiments (Figure S1, see Supporting Information for details). Compound **1**, however, showed high apparent intrinsic clearance in human liver microsomes (HLM)[14] along with inhibition of CYP2C8 and CYP2C9. Although physical properties of the molecule, such as molecular weight (MW), passive permeability (Papp)[15] and LogD,[16] were in a reasonable range, we recognized further attenuation of lipophilicity would most likely be required to improve metabolic stability. This chemical series was highly enabled for parallel chemistry, with a synthetic modularity that made **1** an attractive starting point for further structure-activity relationship (SAR) development. Given the modest potency of **1,** our initial efforts were centered on rapid improvements measured by increased LipE.

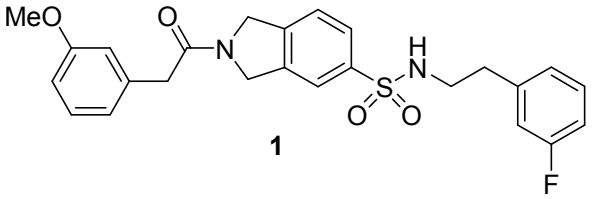

1

- $LogD_{7.4}$ 3.6 / LipE 2.6[a] / MW 469
- HLM Cl_{int} > 320 μL/min/mg[b]
- P_{app} = 8 x10^{-6} cm/s[c]
- Inhibition of CYP2C8 (29%) CYP2C9 (35%)[d]

	MGAT3	MGAT1	MGAT2	DGAT1	DGAT2
IC_{50} (pIC_{50} ± SD)[e]	682 nM (6.2 ± 0.2)	> 40 μM	30 μM (4.5 ± 0.3)	31 μM (4.5 ± 0.2)	> 40 μM

Figure 1. Structure and profile of the HTS hit **1**. [a]LipE, a measure of lipophilic efficiency, is the difference between pIC_{50} and LogD. [b]Human liver microsome clearance. [c]Passive permeability was assessed in Ralph Russ canine kidney cells (RRCK). [d]CYP450 inhibition was assessed at 3 μM. [e]Potency is reported as an IC_{50} with pIC_{50} ± SD in parentheses. IC_{50} values are mean values of at least 3 replicates. Each individual IC_{50} value is generated from an 11 point dose-response curve run in triplicate.

Hit Optimization. The synthesis of 2-(2-(3-methoxyphenyl)acetyl)isoindoline-5-sulfonamides **6a-e** is outlined in Scheme 1. Nucleophilic addition of varied amines (**3a-e**) to 2-(2,2,2-trifluoroacetyl)isoindoline-5-sulfonyl chloride (**2**) under basic conditions, afforded 2-(2,2,2-trifluoroacetyl)isoindoline-5-sulfonamides (**4a-e**). Subsequent deprotection and coupling of 2-(3-methoxyphenyl)acetic acid using HATU, afforded the desired 2-(2-(3-methoxyphenyl)acetyl)isoindoline-5-sulfonamides (**6a-e**). Using this general procedure in both library and singleton format, it was possible to explore the sulfonamide region of the molecule readily.

Scheme 1. Synthesis of isoindoline-5-sulfonamides.

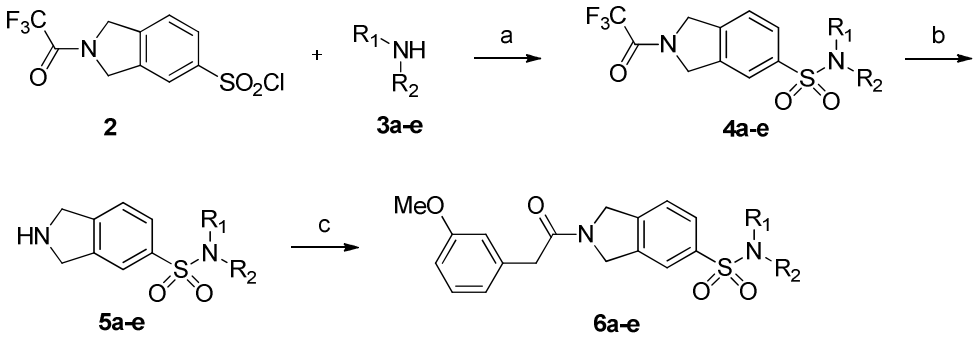

[a]Et_3N, THF, 40 °C *or* pyridine, CH_2Cl_2, 0 °C to 30 °C. [b]K_2CO_3, MeOH *or* NaOH, MeOH/H_2O, 40 °C. [c]2-(3-methoxyphenyl)acetic acid, HATU, *i*Pr_2NEt, DMF.

Key examples from the SAR scan can be found in Table 1. The acidic hydrogen of the sulfonamide appeared important for inhibition, as the methylated variant (**6a**) showed a 4-fold drop in potency compared to the HTS hit **1**. As such, a variety of primary (R_1 = H) instead of secondary amines (**3**) were utilized in our first combinatorial library. In addition, we chose R_2 moieties with reduced lipophilicity when compared to the 3-fluorophenethyl of **1**, targeting analogues with LogD < 2 as part of a strategy to reduce metabolic clearance.

Table 1. *In vitro* potency for MGAT3 inhibition, physicochemical properties and ADME properties for sulfonamides **6a**−**6i**.[17]

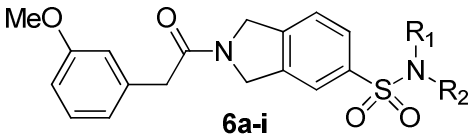

6a-i

Cpd	R_1	R_2	MGAT3 IC_{50} (nM) ($pIC_{50} \pm SD$)	$LogD_{7.4}$	LipE	HLM Cl_{int} (μL/min/mg)	P_{app} (10^{-6} cm/s)
6a	CH_3	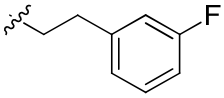	2740 (5.6 ± 0.1)	3.9	1.7	>320	4
6b	H	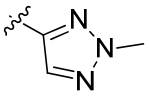	3837 (5.4 ± 0.2)	0.2	5.2	<8	1
6c	H	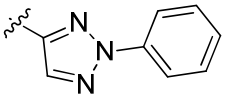	6 (8.2 ± 0.2)	2.3	5.9	273	15
6d	H	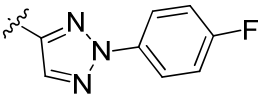	6 (8.2 ± 0.2)	2.5	5.7	13	6
6e	H	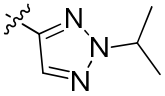	597 (6.2 ± 0.2)	1.4	4.8	<8	25
6f	H	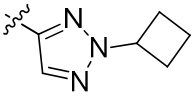	92 (7.0 ± 0.4)	1.7	5.3	22	12
6g	H	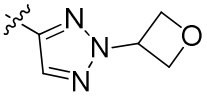	365 (6.4 ± 0.1)	0.2	6.2	<8	3
6h	H	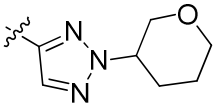	72 (7.1 ± 0.2)	0.9	6.2	<8	5
6i	H	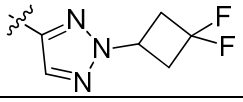	63 (7.2 ± 0.2)	1.5	5.7	<8	7

Triazole **6b** was the only analog from this initial library to show MGAT3 inhibition with an IC_{50} value of less than 10 μM (other analogues not shown). Although the potency of **6b** was significantly attenuated (IC_{50} = 3837 nM) compared to that of **1**, the overall LipE was vastly

improved (5.2 vs. 2.6) as was the metabolic stability (HLM < 8.0 μL/min/mg) suggesting that further modifications of this triazole side chain could offer advantages in balancing the desired properties.

Analogues with substitution at the N2-position of the 1,2,3-triazole showed significant improvement in potency. In particular compound **6c**, showed an approximately 100-fold improvement in potency over the initial hit **1** with superior LipE (5.9 vs. 2.6). However, despite significantly lower LogD, **6c** showed inhibition of CYP2C8 (48%) and CYP2C9 (88%) at 3 μM, and was rapidly metabolized in HLM.

In order to address the microsomal instability of **6c**, its metabolic process was investigated at a molecular level. Metabolite identification studies utilizing human hepatocytes indicated that the phenyl substituent on the triazole is the main site of oxidation. Assessment of various isoforms of CYP450 revealed an important contribution of the CYP2C9 isoform. Virtual docking of **6c** in the X-ray crystal structure of CYP2C9[18] predicted the isoindoline core to bind to the enzyme via hydrophobic interactions, and the acidic sulfonamide to be involved in an ionic interaction with arginine 108 (R108, Figure 2). In this orientation, the pendant phenyl ring can access the heme in an energetically favorable orientation for oxidation, potentially leading to the main human metabolite identified.

Based on this binding model in CYP2C9, a blocking strategy was pursued which led to metabolically stable analogues such as **6d**. Similar to **6c**, 4-fluorophenyl analogue **6d** was potent for MGAT3 inhibition but also demonstrated significant inhibition of CYP2C8 (62%) and CYP2C9 (95%) at 3 μM. We hypothesized that smaller substituents on the triazole would be located further away from the heme core and potentially result in reduced rates of oxidation and

inhibition. Indeed, *i*-propyl substitution (**6e**) proved beneficial for human liver microsomal stability, but this improvement was achieved at the expense of potency.[19]

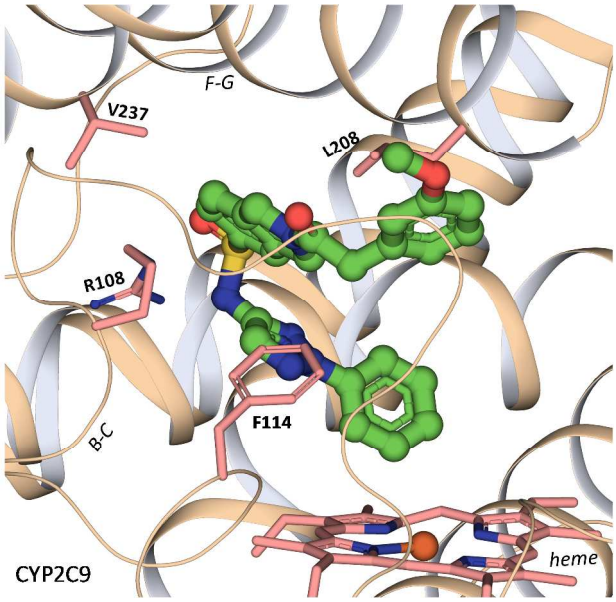

Figure 2. Virtual docking of **6c** in a model of CYP2C9. The structure used for the modeling was PBD ID 1R9O.

Due to their limited availability and diversity, a new procedure for the synthesis and use of N2-substituted triazole building blocks with non-aromatic side chains was developed. As shown in Scheme 2, a selective N2-triazole alkylation was performed on 4,5-dibromo-2H-1,2,3-triazole (**7**).[20] Either base-mediated alkylation with halide (**8**) or Mitsunobu displacement with alcohol (**10**) selectively afforded 4,5-dibromo-2-alkyl-2H-1,2,3-triazoles (**9f-h**). We found that if analogous chemistry was performed on 4-bromo-2H-1,2,3-triazole, we obtained a mixture of N1- and N2-substituted products in favor of the undesired N1-regiochemistry. A metal halogen exchange of **9f-h**, followed by acidic quench, afforded the corresponding 4-bromo-2-alkyl-2H-

1,2,3-triazoles (**11f-h**). Bromotriazoles **11f-i** were subsequently coupled directly with **6j** under copper-mediated conditions.

Scheme 2. Synthesis of N2-substituted triazoles and sulfonamides **6f-i**.

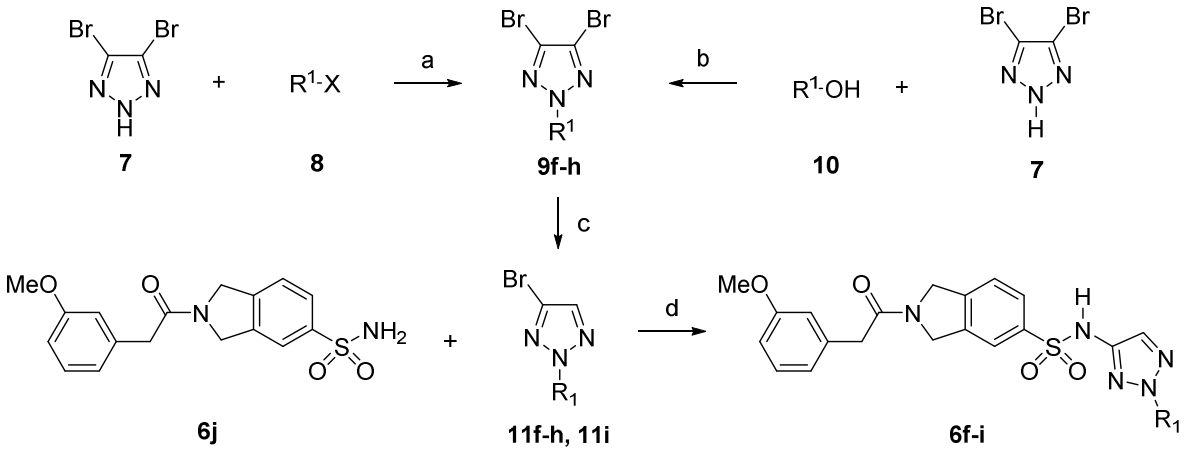

[a]Cs_2CO_3, DMF 120 °C *or* Cs_2CO_3 MeCN 80 °C . [b]DIAD, PPh_3, NEt_3, THF, -78 °C to 30 °C. [c]*i*PrMgCl, THF -20 °C or *t*-BuLi, THF, -78 °C. [d]CuI, K_2CO_3, *trans*-N,N-dimethylcyclohexane-1,2-diamine, DMF, 100 °C.

Using this synthetic sequence, analogues with small alkyl substituent on the triazole were prepared and evaluated for MGAT3 inhibition. A more efficient use of lipophilicity was achieved with small alkyl rings such as *c*-butyl (**6f**), providing potent MGAT3 inhibition (IC_{50} = 92 nM) with low predicted clearance. Assuming the mode of metabolism and binding in CYP2C9 is conserved with **6f**, blocking the distal position of the *c*-butyl ring would prevent oxidative metabolism via CYP2C9. As such, no turnover was detected in human liver microsomes for **6g** and **6i**. Despite its modest potency (IC_{50} = 365 nM), the less lipophilic oxetane analogue **6g** provided comparable lipophilic efficiency (LipE = 6.2). With the goal of increasing the lipophilic character of **6g** to gain potency, tetrahydropyran analogue **6h** was

prepared, which proved to be as efficient (LipE = 6.2) with good potency, low lipophilicity and no observable turnover in HLM.

Since the X-ray crystallographic structure of MGAT3 is not available, the specific interactions of the methoxybenzyl moiety with the enzyme are unknown. All efforts to remove, replace or modify this group were unsuccessful. For instance, alteration of shape, polarity, and size by replacing the methoxybenzyl moiety with a variety of isosteres resulted in significant decreases in MGAT3 potency (see Table S1 for examples), which suggests an important interaction between the protein and this region of the molecule.

In summary, optimization of the sulfonamide region of hit **1** from a HTS led to the identification of high quality, potent and selective MGAT3 inhibitors, which possessed desirable physicochemical properties and *in vitro* PK profiles. The balance of desirable properties was best realized in analogs such as **6f**, **6h** and **6i**.

Determination of IC_{50} values for MGAT3 Inhibition in Cell-Based Assay. We next assessed MGAT3 inhibitors in a cell-based assay using a stable HEK-293 cell line expressing human MGAT3, and measured the incorporation of [^{14}C]-glycerol into TAG. As previously reported, MGAT3 functions as both an MGAT and DGAT enzyme in cultured cells.[12] Under the cell-based assay conditions where MGAT3 is overexpressed, most of the DAG synthesized by MGAT3 is rapidly converted to TAG (data not shown). To ensure TAG generating activity is solely due to MGAT3, cells were treated with MGAT3 inhibitors in the presence of a combination of 3 μM of DGAT1 inhibitor (DGAT1i) PF-04620110 (**12**)[21] and 0.3 μM of DGAT2 inhibitor (DGAT2i) PF- 06424439 (**13**),[7, 22] to completely inhibit DGAT1 and DGAT2.[23] In the cell-based assay under these conditions, **6f** exhibited a typical dose-response curve for a single target inhibition with an IC_{50} value of 205 nM (pIC_{50} = 6.69 ± 0.05) and a Hill

slope of 0.81 (Figure 3). Similar typical single target dose response curves were obtained for **6h** (IC_{50} =760 nM; pIC_{50} = 6.1 ± 0.1) and **6i** (IC_{50} =394 nM; pIC_{50} = 6.41 ± 0.02)[24] with Hill slope values close to 1 (1.1 and 0.87for **6h** and **6i** respectively) in the cell based assay. **6f** showed higher efficacy in cells compared to **6h** and **6i**, which can be at least partially attributed to increased passive permeability of **6f** (Table 1).

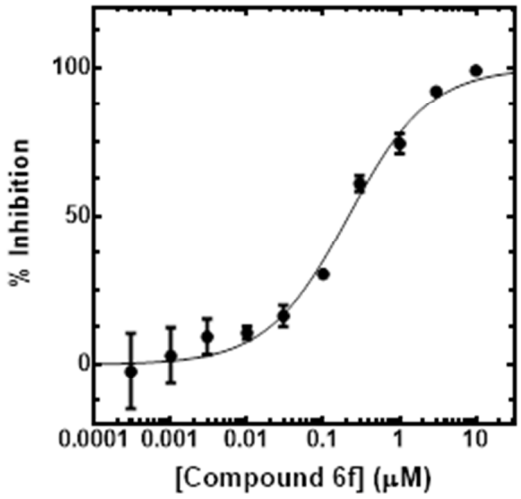

Figure 3. MGAT3 inhibition by **6f** in cell-based assay. HEK-293 cells stably expressing human MGAT3 were treated with **6f** in the presence of DGAT1i **12** and DGAT2i **13** under the conditions where DGAT1 and DGAT2 are completely inhibited as described under Experimental Section.

***In Vitro* Safety and Pharmacokinetic Profiles of 6f.** Compound **6f** showed a clean *in vitro* safety profile with no significant inhibition of the hERG channel or major human CYP450s (CYP1A2, CYP2C8, CYP2C9, CYP2D6, CYP3A4). No genetic toxicology risks were identified, with negative findings in Ames mutagenicity assay and *in vitro* micronucleus assay and no toxicity was observed in HepG2 cells at concentrations up to 300 μM with 72 hour incubation. **6f**

exhibited >160 fold *in vitro* selectivity for MGAT3 over DGAT1, DGAT2, MGAT1 and MGAT2. In addition, as shown in Table S2, **6f** at 10 μM was selective against a broad panel of more than 120 individual targets, including various transporters, receptors, ion channels and enzymes.[25] Based on its *in vitro* profile, **6f** appeared to be a suitable tool compound for *in vivo* experiments and was advanced to PK evaluation. As determined with a 1 mg/kg intravenous dose, **6f** demonstrated low *in vivo* systemic clearance (1.4 mL/min/kg), low volume of distribution (0.17 L/kg) and short effective half-life (1.4 h). When orally dosed in mice, at 5 mg/kg using 0.5% methylcellulose as the vehicle, **6f** exhibited high oral bioavailability of 74% (C_{max} = 9.3 μg/mL, AUC_{last} = 27 μg·h/mL).

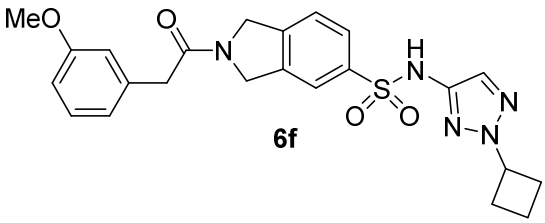

- $LogD_{7.4}$ 1.7 / LipE 5.3 / MW 468
- HLM Clint < 22 μL/min/mg
- Papp = 13 x10^{-6} cm/s

	MGAT3	MGAT1	MGAT2	DGAT1	DGAT2
IC_{50} (pIC_{50}± SD)	92 nM (7.0 ± 0.4)	14.9 μM[a] (4.83 ± 0.09)	19.8 μM[a] (4.70 ± 0.06)	> 50 μM	> 100 μM

Figure 4. *In vitro* profile of optimized MGAT3 inhibitor **6f**. [a]IC_{50} values are mean of 2 replicates.

***In Vivo* Inhibition of MGAT3.** As previously mentioned, MGAT3 is uniquely expressed in humans and higher mammals, but not in rodents. To assess *in vivo* MGAT3 inhibition by **6f**, mice expressing the human *MOGAT3* transgene were generated (termed as hMGAT3 mice). As verified by quantitative real time PCR, expression profile of the human *MOGAT3* transgene in mice was similar to that reported for humans[12] in the small intestine, colon, kidney and liver (Figure S3).[26] Incorporation of uniformly deuterium labeled glycerol into TAG was utilized as

described previously[27] to assess TAG-synthesizing enzyme activity in these mice as well as wild type (WT) mice (see Supporting Information for details on TG analysis). In order to better understand the contribution of MGAT3 to TAG synthesis, mice were pre-treated with an oral administration of **6f** (200 mg/kg) alone or in the presence of DGAT1i **12** and DGAT2i **13**, at 10 and 30 mg/kg respectively. The doses for **12** and **13** were previously established for near complete *in vivo* inhibition of their respective target, as these doses provided compound exposure in plasma well above the IC_{50} values determined from enzymatic assays (Figure S2B and S2C). Oral treatment of mice with **6f** at 200 mg/kg also provided free compound exposure in plasma that was several-fold over the IC_{50} value from the enzymatic assay during the course of the experiment (Figure S2A). One hour after the treatment with inhibitor(s), mice were injected with a bolus of D_8-glycerol via the tail vein, and plasma was collected 30 minutes later. Since 3 deuterium atoms are lost during the esterification process, TAG synthesis was measured by changes in incorporation of D_5-glycerol into triolein (18:1, 18:1, 18:1), which is reported as atom percent excess (APE).

As shown in Figure 5A and 5B, D_5-glycerol incorporation into triolein was similar between the wild type and hMGAT3 mice (white bars; 4.01 ± 0.33% in WT versus 4.56 ± 0.37% in hMGAT3 mice). This data potentially indicate that the total level of triolein synthesis is not altered by the additional *MOGAT3* gene as the contribution of other TAG synthesizing enzymes is sufficient for full incorporation of D_5-Glycerol into TAG. Further supporting this hypothesis, in both wild type and hMGAT3 mice, D_5-glycerol incorporation into triolein was not affected by **6f** alone (Figure 5A and 5B; hatched bars). Treatment with DGAT1i and DGAT2i displayed significantly reduced D_5-glycerol incorporation into triolein in both WT and hMGAT3 mice (Figure 5A and 5B; gray bars), however, additional enrichment of the label was detected from the hMGAT3

mice when compared to the WT mice (gray bars; 3.20±0.27% vs 1.75±019%) suggesting additional triolein synthesizing capacity. Treatment with **6f** in the presence of DGAT1i and DGAT2i did not have any effect in WT mice as expected (Figure 5A, black bar) but showed an additional suppression of D_5-glycerol incorporated triolein in hMGAT3 mice (Figure 5B; black bar).

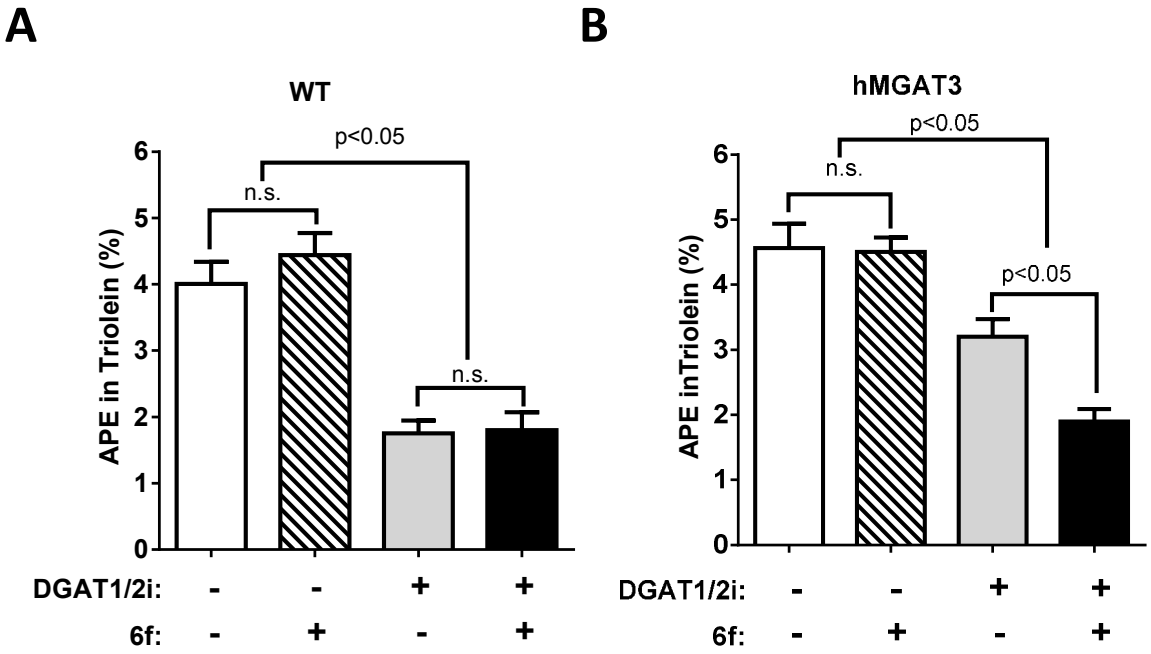

Figure 5. Inhibition of D_5-glycerol incorporation into triolein with **6f** in wild type and hMGAT3 transgenic mice. Wild type and hMGAT3 mice were treated with vehicle (white bar), **6f** (hatched bar), DGAT1i and DGAT2i (gray bar), or **6f** in the presence of DGAT1i and DGAT2i (black bar) one hour prior to a 100 mg/kg tail vein injection of uniformly deuterium labeled glycerol. Blood was collected thirty minutes later and plasma D_5-glycerol incorporation into triolein was measured by LC/MS. Isotopic enrichment in triolein from wild type (**A**) and hMGAT3 mice (**B**) is shown and data are expressed as mean atom percent excess (APE) ± SE. Significance was

determined by two-way Anova and Bonferroni post test. n.s., not statistically significant. n = 6-9 mice per group.

Taken together, these results show that MGAT3 contributes to TAG synthesis in hMGAT3 mouse model and the *in vivo* efficacy of **6f** as a MGAT3 inhibitor was clearly demonstrated in the presence of DGAT1i and DGAT2i. No effect on TAG synthesis by **6f** alone in hMGAT3 mice was measurable (Figure 5B, hatched bar) likely because DGAT1 and 2 activities are sufficient for maximal incorporation of the label into TAG.

CONCLUSION

Sulfonamide **1** was identified from a high-throughput screen as a selective and reversible inhibitor of MGAT3 with relatively high lipophilicity and human liver microsomal intrinsic clearance. LipE-focused optimization of the sulfonamide substituent led to more efficient substituted triazoles such as **6c**. Identification of CYP2C9 as a main isoform for metabolism, metabolites identification and virtual docking of **6c** in the CYP2C9 crystal structure facilitated the optimization of metabolic stability for the series. This led us to explore smaller alkyl substituents on the triazole ring which generated highly efficient MGAT3 inhibitors with improved *in vitro* PK and safety profiles. In summary, our compound optimization efforts provided high quality, small molecule MGAT3 inhibitors such as **6f (PF-06471553)** which displayed suitable PK properties in mouse and *in vivo* MGAT3 inhibition in a transgenic mouse model. The availability of a potent and selective chemical tool and a humanized mouse model described in this report should facilitate further dissection of the physiological function of MGAT3 and its role in lipid homeostasis.

EXPERIMENTAL SECTION

Materials and Methods. All chemicals, reagents, and solvents were purchased from commercial sources and used without further purification unless otherwise noted. ^{1}H NMR spectra were recorded with 400 or 500 MHz spectrometers and are reported relative to residual undeuterated solvent signals. Data for ^{1}H NMR spectra are reported as follows: chemical shift (δ, ppm), multiplicity, coupling constant (Hz), and integration. The multiplicities are denoted as follows: s, singlet; d, doublet; t, triplet; q, quartet; spt, septet; m, multiplet; br s, broad singlet. Mass spectrometry (MS) was performed via atmospheric pressure chemical ionization (APCI) or electrospray ionization (ESI) sources. Liquid chromatography mass spectrometry (LC-MS) was performed on an Agilent 1100 Series (Waters Atlantis C18 column, 4.6 x 50 mm, 5 μm; 95% water/acetonitrile linear gradient to 5% water/acetonitrile over 4 min, hold at 5% water/ 95% acetonitrile to 5.0 min, trifluoroacetic acid modifier (0.05%); flow rate of 2.0 mL/ min). Silica gel chromatography was performed using a medium pressure Biotage or ISCO system and columns prepackaged by various commercial vendors including Biotage and ISCO. Preparative high-performance liquid chromatography (HPLC) purification was performed on a Waters FractionLynx preparative chromatography system using a Phenomenex Gemini/Synergi C18 5μm 150 x 21.2 mm 5μm column and eluting with water and MeCN with (0.1% TFA, formic acid, or NH_4OH) at 30 mL/min for 10 minutes. All tested compounds were determined to be >95% pure by HPLC by UV peak detection at 215 nm. The terms "concentrated", "evaporated" and "evacuated" refer to the removal of solvent at reduced pressure on a rotary evaporator with a water bath temperature not exceeding 60 °C. All procedures and experiments involving animals

were carried as per the protocols and guidelines reviewed and approved by Pfizer Institutional Animal Care and Use Committee

Synthesis. *General Procedure A (Parallel Format)*. Step 1: A solution of the appropriate amine (**3**) (1.0 equiv) in THF (0.25 M) was treated with NEt_3 (1.5 equiv) followed by (2,2,2-trifluoroacetyl)isoindoline-5-sulfonyl chloride (**2**) (1.0 equiv). The reaction was stirred at 40 °C overnight and then evaporated to afford **4**, which was used directly in the next step. Step 2: A solution of compound **4** (1.0 equiv) in MeOH (0.25 M) was treated with K_2CO_3 (5.0 equiv) and stirred at 30 °C overnight and then evaporated to afford **5**, which was used directly in the next step. Step 3: A solution of compound **5** (1.0 equiv) in DMF (0.25 M) was treated with 2-(3-methoxyphenyl)acetic acid (1.2 equiv) and *i*Pr_2EtN (3.0 equiv) followed by HATU (1.5 equiv) and stirred at 30 ^oC overnight and then evaporated to afford **6**, which was purified by preparative HPLC.

*N-(3-fluorophenethyl)-2-(2-(3-methoxyphenyl)acetyl)isoindoline-5-sulfonamide (**1**)*. Prepared according to general procedure A with 2-(3-fluorophenyl)ethanamine. Purified by preparative HPLC (40–60% MeCN: water (0.1% TFA)) to afford **1** (7.0 mg, 14%). ^1H NMR (400 MHz, DMSO-d_6) δ 7.74 (s, 1H), 7.67-7.73 (m, 2H), 7.52 (dd, *J*=8.2, 11.2 Hz, 1H), 7.20–7.30 (m, 2H), 6.95–7.01 (m, 3H), 6.84–6.88 (m, 2H), 6.81 (d, *J*=7.6 Hz, 1H), 4.94 (d, *J*=7.0 Hz, 2H), 4.71 (d, *J*=3.5 Hz, 2H), 3.74 (d, *J*=1.2 Hz, 3H), 3.73 (d, *J*=4.7 Hz, 2H), 3.00 (q, *J*=7.0 Hz, 2H), 2.69 (dt, *J*=2.4, 7.3 Hz, 2H); *m/z* = 469.1 $[M+H]^+$.

*N-(3-fluorophenethyl)-2-(2-(3-methoxyphenyl)acetyl)-N-methylisoindoline-5-sulfonamide (**6a**).* Prepared according to general procedure A with 2-(3-fluorophenyl)-N-methylethanamine (**3a**).

Purified by preparative HPLC (20–100% MeCN: water (0.1% NH_4OH)) to afford **6a** (7.1 mg, 15%). *m/z* = 483.2 $[M+H]^+$.

*2-(2-(3-methoxyphenyl)acetyl)-N-(2-methyl-2H-1,2,3-triazol-4-yl)isoindoline-5-sulfonamide (**6b**)*. Prepared according to general procedure A with 2-methyl-2H-1,2,3-triazol-4-amine (**3b**). Purified by preparative HPLC (20–50% MeCN: water (0.1% formic acid)) to afford **6b** (3.2 mg, 7%). *m/z* = 428.0 $[M+H]^+$.

*2-(2-(3-Methoxyphenyl)acetyl)-N-(2-phenyl-2H-1,2,3-triazol-4-yl)isoindoline-5-sulfonamide (**6c**)*. Step 1: A 0 °C solution of 2-phenyl-2H-1,2,3-triazol-4-amine (**3c**) (214 mg, 1.34 mmol) and anhydrous pyridine (200 µL, 2.48 mmol) in CH_2Cl_2 (3 mL) was treated with a solution of (2,2,2-trifluoroacetyl)isoindoline-5-sulfonyl chloride (**2**) (400 mg, 1.28 mmol) in CH_2Cl_2 (3 mL) in a dropwise fashion. The reaction was warmed to room temperature overnight. The reaction was diluted with CH_2Cl_2 (30 mL) and washed with saturated aqueous NH_4Cl (30 mL). The organic layer was dried over Na_2SO_4 and concentrated under reduced pressure. The crude material was purified by silica gel column chromatography (15–70% EtOAc/Heptanes) to afford **4c** (526 mg, 94%) as a white solid. ^1H NMR (400 MHz, DMSO-d_6) δ 11.49 (s, 1H), 7.95 (d, *J*=15.1 Hz, 1H), 7.80–7.89 (m, 4H), 7.56–7.64 (m, 1H), 7.52 (t, *J*=8.1 Hz, 2H), 7.34–7.41 (m, 1H), 5.08 (d, *J*=5.4 Hz, 2H), 4.87 (d, *J*=6.8 Hz, 2H); m/z = 438.2 $[M+H]^+$. Step 2: A solution of **4c** (16 mg, 0.04 mmol) in MeOH/water (1 mL/500 µL) was treated with sodium hydroxide (46 µL, 0.19 mmol, 4N) and heated to 40 °C for 1 hour. The reaction was cooled and the MeOH evacuated. The remaining aqueous solution was cooled to 0 °C and acidified to pH=8 with 3N HCl. The reaction was evacuated to afford crude **5c** which was carried forward directly. Step 3: To a solution of **5c** (13.0 mg, 0.04 mmol) in DMF (1 mL) was added 2-(3-methoxyphenyl)acetic

acid (6.30 mg, 0.04 mmol) and *i*Pr_2EtN (20 μL, 0.11 mmol), followed by HATU (16.0 mg, 0.04 mmol). The reaction was stirred at room temperature overnight and then evacuated and purified by preparative HPLC (40–60% MeCN: water (0.1% TFA)) to afford the title compound **6c** (7.6 mg, 40%) as a white solid. ^{1}H NMR (400 MHz, DMSO-d_6) δ 11.44 (s, 1H), 7.90 (d, *J*=20.3 Hz, 1H), 7.78–7.86 (m, 4H), 7.50–7.60 (m, 3H), 7.39 (ddd, *J*=1.2, 7.3, 14.9 Hz, 1H), 7.21 (t, *J*=8.1 Hz, 1H), 6.78–6.87 (m, 3H), 4.94 (d, *J*=6.8 Hz, 2H), 4.70 (d, *J*=8.5 Hz, 2H), 3.73 (d, *J*=2.0 Hz, 3H), 3.70 (s, 2H); m/z = 490.2 $[M+H]^+$.

*N-(2-(4-fluorophenyl)-2H-1,2,3-triazol-4-yl)-2-(2-(3-methoxyphenyl)acetyl)isoindoline-5-sulfonamide (**6d**)*. Prepared in analogous fashion to **6c**, with 2-(4-fluorophenyl)-2H-1,2,3-triazol-4-amine (**3d**). Purified by preparative HPLC (50–80% MeCN: water (0.1% formic acid)) to afford **6d** (7.3 mg, 7%). ^{1}H NMR (400 MHz, $CDCl_3$) δ 7.72–7.84 (m, 5H), 7.31–7.41 (m, 1H), 7.09–7.13 (t, *J*=9.2 Hz, 3H), 6.86–6.88 (m, 2H), 6.78–6.80 (m, 1H), 4.83 (s, 2H), 4.80 (s, 2H), 3.78 (s, 3H), 3.72 (s, 2H); m/z = 508.3 $[M+H]^+$.

*N-(2-isopropyl-2H-1,2,3-triazol-4-yl)-2-(2-(3-methoxyphenyl)acetyl)isoindoline-5-sulfonamide (**6e**)*. Prepared according to general procedure A with 2-isopropyl-2H-1,2,3-triazol-4-amine. Purified by preparative HPLC (5–95% MeCN: water (0.1% NH_4OH)) to afford **6e** (5.1 mg, 11%). *m/z* = 456.1 $[M+H]^+$.

*N-(2-cyclobutyl-2H-1,2,3-triazol-4-yl)-2-(2-(3-methoxyphenyl)acetyl)isoindoline-5-sulfonamide (**6f**)*. A mixture of 2-(2-(3-methoxyphenyl)acetyl)isoindoline-5-sulfonamide (**6j**) (7.27 g, 21.0 mmol), 4-bromo-2-cyclobutyl-2H-1,2,3-triazole (**11f**) (4.20 g, 21.0 mmol), *trans*-N,N-dimethylcyclohexane-1,2-diamine (1.70 g, 12.0 mmol), CuI (185 mg, 5.25 mmol) and K_2CO_3 (6.62 g, 48.0 mmol) in DMF (160 mL) was stirred at 100 °C overnight. The reaction mixture

was cooled and filtered through Celite. The filtrate was poured into water (150 mL) and extracted with CH_2Cl_2 (3 x 150 mL). The organics were combined, dried over Na_2SO_4 and concentrated. The crude material was purified by silica gel column chromatography (80–85% EtOAc/petroleum ether) to afford the title compound **6f** (6.80 g, 69%) as a white solid. ^{1}H NMR (400 MHz, DMSO-d_6) δ 11.01 (s, 1H), 7.80 (d, *J*=15.6 Hz, 1H), 7.72 (m, 1H), 7.55 (t, *J*=6.8, 1H), 7.48 (s, 1H), 7.23 (t, *J*=8.0, 1H), 6.80–6.81-(m, 3H), 4.97–4.94 (m, 3H), 4.70 (s, 2H), 3.74 (s, 3H), 3.72 (s, 2H), 2.34–2.38 (m, 4H), 1.77–1.80 (m, 2H); m/z = 468.0 $[M+H]^+$.

*2-(2-(3-methoxyphenyl)acetyl)-N-(2-(oxetan-3-yl)-2H-1,2,3-triazol-4-yl)isoindoline-5-sulfonamide (**6g**)*. Prepared in analogous fashion to **6f**, with 4-bromo-2-(oxetan-3-yl)-2H-1,2,3-triazole (**11g**). Purified by preparative HPLC (30–50% MeCN: water (0.1% formic acid)) to afford **6g** (10.6 mg, 7%). ^{1}H NMR (400 MHz, DMSO-d_6) δ 7.80–7.68 (m, 2H), 7.53–7.43 (m, 2H), 7.23–7.19 (t, *J*=8.0 Hz, 1H), 6.83–6.79 (m, 3H), 5.65–5.14 (m, 2H), 4.96–4.87 (m, 3H), 4.76 (t, *J*=6.4 Hz, 1H), 4.68–4.66 (m, 2H), 4.43 (s, 1H), 3.72 (s, 3H), 3.70 (s, 2H); m/z = 492.1 $[M+Na]^+$.

*2-(2-(3-methoxyphenyl)acetyl)-N-(2-(tetrahydro-2H-pyran-4-yl)-2H-1,2,3-triazol-4-yl)isoindoline-5-sulfonamide (**6h**)*. Prepared in analogous fashion to **6f**, with 4-bromo-2-(tetrahydro-2H-pyran-4-yl)-2H-1,2,3-triazole (**11h**). Purified by preparative HPLC (15–45% MeCN: water (0.1% formic acid)) to afford **6h** (18.0 mg, 17%). ^{1}H NMR (400 MHz, MeOH-d_4) δ 7.49–7.79 (m, 2H), 7.44–7.47 (m, 2H), 7.24 (t, *J*=6.8 Hz, 1H), 6.87–6.89 (m, 2H), 6.82 (d, *J*=8.4 Hz, 1H), 4.93 (d, *J*=6.4 Hz, 2H), 4.80 (d, *J*=5.6 Hz, 2H), 4.47–4.51 (m, 1H), 3.91–3.95 (m, 2H), 3.78 (m, 5H), 3.48–3.55 (m, 2H), 1.96–2.01 (m, 4H); m/z = 497.9 $[M+H]^+$.

*N-(2-(3,3-difluorocyclobutyl)-2H-1,2,3-triazol-4-yl)-2-(2-(3-methoxyphenyl)acetyl)isoindoline-5-sulfonamide (**6i**)*. Prepared in analogous fashion to **6f**, with 4-bromo-2-(3,3-difluorocyclobutyl)-2H-1,2,3-triazole (**11i**). Purified by preparative HPLC (35–45% MeCN: water (0.1% formic acid)) to afford **6i** (12.9 mg, 18%). ^{1}H NMR (400 MHz, MeOH-d_4) δ 7.75–7.82 (m, 2H), 7.52 (s, 1H), 7.46 (dd, *J*=8.4, 15.2 Hz, 1H), 7.23 (t, *J*=7.2 Hz, 1H), 6.86–6.88 (m, 2H), 6.81 (d, *J*=8.8 Hz, 1H), 4.92 (s, 2H), 4.79 (s, 2H), 3.77 (s, 5H), 3.07–3.12 (s, 4H); m/z = 504.2 $[M+H]^+$.

Determination of IC_{50} Values for MGAT3 and DGAT2 Inhibition. Enzyme activity for MGAT3 and DGAT2 was determined by measuring the incorporation of the [1-^{14}C]decanoyl moiety into triacylglycerol using [1-^{14}C]decanoyl-CoA (50 mCi/mmol, Perkin Elmer, Waltham , MA) and 1,2-didecanoyl-*sn*-glycerol (Avanti Polar Lipids, Alabaster, AL) as substrates. The MGAT3 reactions were carried out in 384-well white Polyplates (Perkin Elmer, Waltham, MA) in a total volume of 20 µL. To 1 µL of compounds dissolved in dimethylsulfoxide (DMSO) and spotted at the bottom of each well, 15 µL of the detergent-solubilized MGAT3 membrane fraction (0.0033 mg/mL) diluted in 67 mM Hepes-NaOH, pH 7.4, 13.3 mM $MgCl_2$, containing 133.3 nM methyl arachidonyl fluorophosphonate (MAFP, Cayman Chemical, Ann Arbor, MI; dried from ethyl acetate stock solution under argon gas and dissolved in DMSO as 5 mM stock) and 0.013% Triton X-100 was added. After this mixture was preincubated at room temperature for 30 min, MGAT3 reactions were initiated by the addition of 4 µL of substrates containing 10 µM [1-^{14}C]decanoyl-CoA and 175 µM 1,2-didecanoyl-*sn*-glycerol dissolved in 12.5% acetone. The DGAT2 reactions were also carried out in 384-well white Polyplates in a total volume of 20 µL. To 1 µL of compounds dissolved in 100% DMSO and spotted at the bottom of each well, 5 µL of 0.04% bovine serum albumin (BSA, fatty acid free, Sigma Aldrich, ST. Louis, MO) was added and the mixture was kept at room temperature for 20 min. To this mixture, 10 µL of

DGAT2 membrane fraction (0.01 mg/mL) diluted in 100 mM Hepes-NaOH, pH 7.4, 20 mM $MgCl_2$, containing 200 nM MAFP was added. After this mixture was preincubated at room temperature for 120 min, DGAT2 reactions were initiated by the addition of 4 μL of substrates containing 30 μM [1-^{14}C]decanoyl-CoA and 125 μM 1,2-didecanoyl-*sn*-glycerol dissolved in 12.5% acetone. The reaction mixtures for both MGAT3 and DGAT2 were incubated at room temperature for 40 min and the reactions were stopped by addition of 5 μL of 1% H_3PO_4. After the addition of 45 μL MicroScint-E, plates were sealed with Top Seal-A covers and phase partitioning of substrates and products was achieved using a HT-91100 microplate orbital shaker (Big Bear Automation, Santa Clara, CA). Plates were centrifuged at 2,000 x g for 1 min and then were sealed again with fresh covers before reading in a 1450 Microbeta Wallac Trilux Scintillation Counter (Perkin Elmer). MGAT3 and DGAT2 activities were measured by quantifying the generated product [^{14}C]tridecanoylglycerol in the upper organic phase. Background activity obtained using 50 μM (1*R*, 2*R*)-2-({3'-Fluoro-4'-[(6-fluoro-1, 3-benzothiazol-2-yl)amino]-1,1'-biphenyl-4-yl}carbonyl)cyclopentanecarboxylic acid for complete inhibition was subtracted from all reactions (US 20040224997, Example 26). Even though this compound was initially described as a DGAT1 inhibitor,[28] we have found that it inhibits DGAT1, DGAT2, MGAT1, MGAT2, and MGAT3 with IC_{50} values of 0.114 ± 0.012, 1.43 ± 0.30, 0.584 ± 0.15, 1.63 ± 0.14, and 4.39 ± 1.2 μM, respectively, under the assay conditions described by Futatsugi *et al*.[7] Therefore we used 50 μM Example 26 for complete inhibition of all of the aforementioned enzymes.

Inhibitors were tested at eleven different concentrations to generate IC_{50} values for each compound. The eleven inhibitor concentrations employed typically included 50, 15.8, 5, 1.58, 0.50, 0.16, 0.05, 0.016, 0.005, 0.0016, and 0.0005 μM. The data were plotted as percentage of

inhibition versus inhibitor concentration and fit to the equation, $y = 100/[1 + (x/IC_{50})^z]$, where IC_{50} is the inhibitor concentration at 50% inhibition and z is the Hill slope (the slope of the curve at its inflection point, using GraphPad Prism (GraphPad Software, Inc., La Jolla, CA).

MGAT3 Cell-Based Assay. After coating 96-well tissue culture plates with 100 μL of 0.01% ethylene imine polymer solution at room temperature for 30-60 min and then washing them with 200 μL of phosphate-buffered saline (PBS), HEK-293 cells stably expressing human MGAT3 were seeded at 80,000 cells/well in Dulbecco's modified Eagle's medium (DMEM) containing 10% fetal bovine serum (FBS) and 100 μg/mL zeocin. All tissue culture incubations described below were performed at 37 ºC and 5% CO_2. After ~16 hr, the media from each well was removed and replaced with 143.5 μL fresh serum free media containing 0.4 mM dodecanoic acid. After incubating cells at 37 ºC for 40 min, 1.5 μL MGAT3 inhibitor containing DGAT1 and DGAT2 inhibitors (**12** and **13** respectively) to final concentrations of 3 and 0.3 μM, respectively, was added to cells, which were incubated for additional 20 min. After the addition of 5 μL [1,3-^{14}C] glycerol (the stock at 0.1 mCi/mL l and 40 mCi/mmol in 50% EtOH was dried under N_2 and diluted by 2.5-fold with serum free media), cells were further incubated for 3.5 hr. Cell media were removed and replaced with 100 μL of extraction buffer containing 9:1 isopropyl alcohol: tetrahydrofuran (v/v). The plate was placed on a shaker, mixed vigorously for 15 min at room temperature, and centrifuged at 3,000 x g for 5 min. The resulting supernatant (40 μL) was loaded onto TLC plates (20x20 cm) and radioactive lipids were resolved using a 2-solvent system (Solvent 1 contained a 100:100:100:40.2:36.1 mixture of ethyl acetate: isopropyl alcohol: chloroform: methanol: 0.25% potassium chloride; Solvent 2 contained a 70:27:3 hexane: diethyl ether: acetic acid mixture). A 2-solvent system was used to allow better separation of DAG and TAG on TLC. TLC plates were run with solvent 1 until the solvent front reached ~6.5 cm from

the origin and dried under N_2, which then were followed by solvent 2. Radioactive lipids were visualized and quantitated using a Phosphorimager System (Molecular Dynamics). Inhibitors were tested at eleven different concentrations to generate IC_{50} values for each compound. The data were plotted as percentage of inhibition versus inhibitor concentration and fit to the equation, $y = 100/[1 + (x/IC_{50})^z]$, where IC_{50} is the inhibitor concentration at 50% inhibition and z is the Hill slope (the slope of the curve at its inflection point, using GraphPad Prism (GraphPad Software, Inc., La Jolla, CA).

Glycerol Incorporation into TAG in human MGAT3 transgenic mice. All animals were studied in the fed state between 8 AM and 12 PM. The experimental design was modified from a previously published protocol.[27] The morning of the studies, uniformly labeled D_8-glycerol was diluted to 10 mg/mL in saline and compounds were prepared in 0.5% methyl cellulose in saline. Inhibitors were dosed at 200 mg/kg for the MGAT3 inhibitor **6f**, 30 mg/kg for DGAT1 inhibitor **12** and 10 mg/kg for DGAT2 inhibitor **13**. After 1 hour, animals were injected with 100 mg/kg of uniformly labeled D_8-glycerol via tail vein. After 30 minutes, blood was collected in EDTA coated tubes and plasma was separated by centrifugation. 10 μL of plasma was snap frozen in a separate tube for lipid extraction. See Experimental Section in Supporting Information for full details on lipid extraction and LC/MS analysis.

ASSOCIATED CONTENT

Supporting Information. SAR for the amide region, synthesis of key intermediates, methodology for docking in CYP2C9, *in vitro* selectivity of **6f**, reversibility experiment with **1**, *in vitro* selectivity data as well as mouse PK data for **6f**, **12** and **13**, generation of transgenic

animals, analysis of *MOGAT3* gene expression and LC-MS analysis of plasma triglycerides. This material is available free of charge via the Internet at http://pubs.acs.org.

AUTHOR INFORMATION

Corresponding Authors

*E-mail: Kim.Huard@Pfizer.com and Allyn.T.Londregan@Pfizer.com

Funding Sources

All authors were employed by Pfizer during the completion and analysis of the reported studies.

ACKNOWLEDGMENT

The authors would like to thank Jeffrey A. Pfefferkorn, William Esler, Derek M. Erion, Amit Kalgutkar, Nick Verra, Paul Amor, Sylvie Perez, Matthew Gorgoglione and Lisa Brideau for their help with the design and execution of the *in vivo* study and metabolite identification. We would also like to thank Mark Niosi for the rat pharmacokinetic study, Kun Song for his contributions to the chemistry program and Steven Hawrylik and Tracy Brown Phillips for DGAT2 expression.

ABBREVIATIONS

TAG, triacylglycerol; MGAT3, monoacylglycerol acyltransferase 3; MAG, monoacylglycerol; DAG, diacylglycerol; DGAT1, diacylglycerol acyltransferase 1; DGAT2, diacylglycerol acyltransferase 2; T2DM, type 2 diabetes mellitus; NASH, nonalcoholic steatohepatitis; MGATs, monoacylglycerol acyltransferases; DGATs, diacylglycerol acyltransferases; MGAT1, monoacylglycerol acyltransferase 1; MGAT2, monoacylglycerol acyltransferase 2; NAFLD,

nonalcoholic fatty liver disease; LipE, lipophilic efficiency; PK, pharmacokinetic; HTS, high-throughput screening; HLM, human liver microsome; CYP, cytochrome P450; MW, molecular weight; Papp, passive permeability; RRCK, Ralph Russ canine kidney cells; HATU, 1-[Bis(dimethylamino)methylene]-1H-1,2,3-triazolo[4,5-b]pyridinium 3-oxid hexafluorophosphate; DIAD, Diisopropyl azodicarboxylate; DGAT1i, DGAT1 inhibitor; DGAT2i, DGAT2 inhibitor; hMGAT3, transgenic mice; D_5-glycerol, deuterium labeled glycerol; WT, wild type; APE, atom percent excess; HFD, high fat diet; LC-MS, liquid chromatography-mass spectrometry; MAFP, methyl arachidonyl fluorophosphonate.

REFERENCES

(1) a) Unger R. H. Lipotoxic diseases. *Annu. Rev. Med*. **2002**, *53*, 319–336. b) Friedman J. Fat in all the wrong places. *Nature* **2002**, *415*, 268–269. c) Schaffer J. E. Lipotoxicity: when tissues overeat. *Curr. Opin. Lipidol*. **2003**, *14*, 281–287.

(2) a) Shi Y.; Cheng D. Beyond triglyceride synthesis: the dynamic functional roles of MGAT and DGAT enzymes in energy metabolism. *Am. J. Physiol. Endocrinol. Metab*. **2009**, *297*, E10–E18. b) Yen C. L.; Stone S. J.; Koliwad S.; Harris C.; Farese R. V.; Jr Thematic review series: glycerolipids. DGAT enzymes and triacylglycerol biosynthesis. *J. Lipid Res*. **2008**, *49*, 2283–2301.

(3) a) Cases S.; Smith S. J.; Zheng Y. W.; Myers H. M.; Lear S. R.; Sande E.; Novak S.; Collins C.; Welch C. B.; Lusis A. J.; Erickson S. K.; Farese R. V. Jr. Identification of a gene encoding an acyl CoA: diacylglycerol acyltransferase, a key enzyme in triacylglycerol synthesis. *Proc. Natl Acad. Sci. USA* **1998**, *95*, 13018–13023. b) Cases S.; Stone S. J.; Zhou

P.; Yen E.; Tow B.; Lardizabal K. D.; Voelker T.; Farese R. V. Jr. Cloning of DGAT2, a second mammalian diacylglycerol acyltransferase, and related family members. *J. Biol. Chem*. **2001**, *276*, 38870–38876.

(4) a) Cao J.; Lockwood J.; Burn P.; Shi Y. Cloning and functional characterization of a mouse intestinal acyl-CoA: monoacylglycerol acyltransferase, MGAT2. *J. Biol. Chem*. **2003**, *278*, 13860–13866. b) Yen C. L.; Farese R. V. Jr. MGAT2, a monoacylglycerol acyltransferase expressed in the small intestine. *J. Biol. Chem*. **2003**, *278* (28), 18532–18537. c) Cao, J.; Burn, P.; Shi, Y., Properties of the mouse intestinal acyl-CoA:monoacylglycerol acyltransferase, MGAT2. *J. Biol. Chem.* **2003,** *278* (28), 25657–25663. d) Yen C. L.; Stone S. J.; Cases S.; Zhou P.; Farese R. V. Jr. Identification of a gene encoding MGAT1, a monoacylglycerol acyltransferase. *Proc. Natl Acad. Sci. USA* **2002**, *99*, 8512–8517. e) Cheng D.; Nelson T. C.; Chen J.; Walker S. G.; Wardwell-Swanson J.; Meegalla R.; Taub R.; Billheimer J. T.; Ramaker M.; Feder J. N. Identification of acyl coenzyme A: monoacylglycerol acyltransferase 3, an intestinal specific enzyme implicated in dietary fat absorption. *J. Biol. Chem*. **2003**, *278* (16), 13611–13614.

(5) a) DeVita, R. J. and Pinto, S. Current Status of the Research and Development of Diacylglycerol O-Acyltransferase 1 (Dgat1) Inhibitors. *J. Med. Chem.* **2013**, *56*, 9820–9825. b) Dow, R. L. Acyl-Coa: Diacylglycerol Acyltransferase-1 Inhibition as an Approach to the Treatment of Type 2 Diabetes. *RSC Drug Discovery Ser.,* **2012**, *27*, 215–248. c) Birch, A. M.; Buckett, L. K.; Turnbull, A. V. *Curr. Opin. Drug Discovery Dev.* **2010**, *13*, 489.

(6) a) Choi, C. S.; Savage, D. B.; Kulkarni, A.; Yu, X. X.; Liu, Z. X.; Morino, K.; Kim, S.; Distefano, A.; Samuel, V. T.; Neschen, S.; Zhang, D.; Wang, A.; Zhang, X. M.; Kahn, M.; Cline, G. W.; Pandey, S. K.; Geisler, J. G.; Bhanot, S.; Monia, B. P.; Shulman, G. I.,

Suppression of diacylglycerol acyltransferase-2 (DGAT2), but not DGAT1, with antisense oligonucleotides reverses diet-induced hepatic steatosis and insulin resistance. *J. Biol. Chem.* **2007,** *282* (31), 22678–22688. b) Liu, Y.; Millar, J. S.; Cromley, D. A.; Graham, M.; Crooke, R.; Billheimer, J. T.; Rader, D. J., Knockdown of acyl-CoA:diacylglycerol acyltransferase 2 with antisense oligonucleotide reduces VLDL, TG and ApoB secretion in mice. *Biochim. Biophys. Acta* **2008,** *1781* (3), 97–104. c) Yu, X. X.; Murray, S. F.; Pandey, S. K.; Booten, S. L.; Bao, D.; Song, X. Z.; Kelly, S.; Chen, S.; McKay, R.; Monia, B. P.; Bhanot, S., Antisense oligonucleotide reduction of DGAT2 expression improves hepatic steatosis and hyperlipidemia in obese mice. *Hepatology* **2005,** *42* (2), 362–371.

(7) DGAT2 inhibitors, which exhibit robust *in vivo* efficacy including reduction in plasma TAG and total cholesterol, have been recently reported: Futatsugi, K.; Kung, D. W.; Orr, S. T. M.; Cabral, S.; Hepworth, D.; Aspnes, G.; Bader, S.; Bian, J.; Boehm, M.; Carpino, P. A.; Coffey, S. B.; Dowling, M. S.; Herr, M.; Jiao, W.; Lavergne, S. Y.; Li, Q.; Clark, R. W.; Erion, D.; Kou, K.; Lee, K.; Pabst, B. A.; Perez, S. M.; Purkal, J.; Jorgensen, C. C.; Goosen, T. C.; Gosset, J. R.; Niosi, M.; Pettersen, J. C.; Pfefferkorn, J. A.; Ahn, K.; Goodwin, B. Discovery and Optimization of Imidazopyridine-based Inhibitors of Diacylglycerol Acyltransferase 2 (DGAT2). *J. Med.Chem*. companion manuscript submitted.

(8) Yen, C. L.; Cheong, M. L.; Grueter, C.; Zhou, P.; Moriwaki, J.; Wong, J. S.; Hubbard, B.; Marmor, S.; Farese, R. V., Jr. Deficiency of the intestinal enzyme acyl CoA:monoacylglycerol acyltransferase-2 protects mice from metabolic disorders induced by high-fat feeding. *Nat. Med.* **2009,** *15* (4), 442–446.

(9) a) Barlind, J. G.; Buckett, L. K.; Crosby, S. G.; Davidsson, Ö.; Emtenäs, H.; Ertan, A.; Jurva, U.; Lemurell, M.; Gutierrez, P. M.; Nilsson, K.; O'Mahony, G.; Petersson, A. U.; Redzic, A.;

Wågberg, F.; Yuan, Z.-Q. Identification and design of a novel series of MGAT2 inhibitors. *Bioorg. Med. Chem. Lett.* **2013**, *23*, 2721-2726. b) Scott, J. S.; Berry, D. J.; Brown, H. S.; Buckett, L.; Clarke, D. S.; Goldberg, K.; Hudson, J. A.; Leach, A. G.; MacFaul, P. A.; Raubo, P.; Robb, G. Achieving improved permeability by hydrogen bond donor modulation in a series of MGAT2 inhibitors. *Med. Chem. Comm.* **2013**, *4*, 1305-1311. c) Sato, K.; Takahagi, H.; Yoshikawa, T.; Morimoto, S.; Takai, T.; Hidaka, K.; Kamaura, M.; Kubo, O.; Adachi, R.; Ishii, T.; Maki, T.; Mochida, T.; Takekawa, S.; Nakakariya, M.; Amano, N.; Kitazaki, T. Discovery of a Novel Series of N-Phenylindoline-5-sulfonamide Derivatives as Potent, Selective, and Orally Bioavailable Acyl CoA:Monoacylglycerol Acyltransferase-2 Inhibitors. *J. Med. Chem.* **2015**, *58*, 3892-3909.

(10) Cao J.; Cheng L.; Shi Y. Catalytic properties of MGAT3, a putative triacylgycerol synthase. *J. Lipid Res*. **2007**, *48*, 583–591.

(11) Stone, S. J.; Levin, M. C.; Farese, R. V., Jr., Membrane topology and identification of key functional amino acid residues of murine acyl-CoA:diacylglycerol acyltransferase-2. *J. Biol. Chem.* **2006,** *281* (52), 40273–40282.

(12) Hall, A. M.; Kou, K.; Chen, Z.; Pietka, T. A.; Kumar, M.; Korenblat, K. M.; Lee, K.; Ahn, K.; Fabbrini, E.; Klein, S.; Goodwin, B.; Finck, B. N. Evidence for regulated monoacylglycerol acyltransferase expression and activity in human liver. *J. Lipid Res*. **2012**, *53*, 990–999.

(13) Edwards, M. P.; Price, D. A. Role of Physicochemical Properties and Ligand Lipophilicity Efficiency in Addressing Drug Safety Risks. *Annu. Rep. Med. Chem*. **2010**, *45*, 380–391.

(14) Obach, R. S. The Prediction of Human Clearance from Hepatic Microsomal Metabolism Data. *Curr. Opin. Drug Discovery Dev*. **2001**, *4*, 36–44.

(15) Passive permeability was assessed in Ralph Russ canine kidney cells: Di, L.; Whitney-Pickett, C.; Umland, J. O.; Zhang, H.; Zhang, X.; Gebhard, D. F.; Lai, Y.; Federico, J. J.; Davidson, R. E.; Smith, R.; Reyner, E. L.; Lee, C.; Feng, B.; Rotter, C.; Varma, M. V.; Kempshall, S.; Fenner, K.; El-Kattan, A. F.; Liston, T. E.; Troutman, M. D. Development of a New Permeability Assay Using Low-Efflux MDCKII Cells. *J. Pharm. Sci*. **2011**, *100*, 4974–4985.

(16) LogD values were determined using the shake-flask method with an octanol:water partition at pH 7.4. The assay method was adapted from published protocol using MS rather than HPLC for sample analysis: Hay, T.; Jones, R.; Beaumont, K.; Kemp, M. Modulation of the Partition Coefficient between Octanol and Buffer at Ph 7.4 and pKa to Achieve the Optimum Balance of Blood Clearance and Volume of Distribution for a Series of Tetrahydropyran Histamine Type 3 Receptor Antagonists. *Drug Metab. Dispo*. **2009**, *37*, 1864-1870.

(17) All compounds in Table 1 were inactive in the DGAT2 assay with the exception of **6d** which had an IC_{50} of 12.3 μM (n=1).

(18) Methodology for CYP2C9 docking is described in the supporting information. Also, see a) Sun, H.; Bessire, A.J.; Vaz, A. Dirlotapide as a model substrate to refine structure-based drug design strategies on CYP3A4-catalyzed metabolism. *Bioorg. Med. Chem. Lett*. **2012**, *22*, 371–6. b) Sun, H.; Scott, D.O. Metabolism of 4-Aminopiperidine Drugs by Cytochrome P450s: Molecular and Quantum Mechanical Insights into Drug Design. *ACS Med. Chem. Lett*. **2011**, *2*, 638–643. For CYP2C9 crystal structure (PBD ID: 1R9O), see Wester, M. R.;

Yano, J. K.; Schoch, G. A.; Yang, C.; Griffin, K. J.; Stout, C. D.; Johnson, E. F. The structure of human cytochrome P450 2C9 complexed with flurbiprofen at 2.0-A resolution. *J. Biol. Chem*. **2004**, *279*, 35630–7.

(19) Pairwise analysis suggests this improvement is not driven only by decreased lipophilicity. See Sun, H.; Keefer, C. E.; Scott, D. O. Systematic and pairwise analysis of the effects of aromatic halogenation and trifluoromethyl substitution on human liver microsomal clearance. *Drug. Metab. Lett*. **2011**, *5*, 232–42.

(20) Wang, X.; Zhang, L.; Krishnamurthy, D.; Senanayake, C. H.; Wipf, P. General solution to the synthesis of *N*-2-substituted 1,2,3-triazoles. *Org. Lett.*, **2010**, *12*, 4632–4635.

(21) Dow, R. L.; Andrews, M. P.; Li, J.-C.; Gibbs, E. M.; Guzman-Perez, A.; LaPerle, J. L.; Li, Q.; Mather, D.; Munchhof, M. J.; Niosi, M.; Patel, L.; Perreault, C.; Tapley, S.; Zavadoski, W. Defining the key pharmacophore elements of PF-04620110: Discovery of a potent, orally-active, neutral DGAT-1 inhibitor. *Bioorg. Med. Chem*. **2013**, *21*, 5081–5097.

(22) Ahn, K.; Boehm, M.; Cabral, S.; Carpino, P. A.; Futatsugi, K.; Hepworth, D.; Kung, D. W.; Orr, S.; Wang, J. Preparation of Pyrrolidinylimidazopyridinylpiperidinylmethanone Derivatives and Analogs for use as Diacylglycerol Acyltransferase 2 Inhibitors. WO13150416; 2013.

(23) See Table S3 for *in vitro* potency and selectivity data for **6f**, **12** and **13** against the acyltransferases of interest. Detailed protocol for cell-based assay can be found in the Experimental Section.

(24) Potency is reported as an IC_{50} with $pIC_{50} \pm SD$. IC_{50} values are means of at least 3 replicates for **6f** and **6i**, and 2 replicates for **6h**.

(25) The only target from the selectivity panel for which **6f** showed significant effect was peroxisome proliferator activated receptor gamma (PPAR gamma) with an IC_{50} value of 4 μM. We believe this does not affect the results from the *in vivo* study described in this manuscript as the maximal free concentration of **6f** does not reach this level (Figure 2A). Additionally, the effects of PPAR gamma activation or inhibition would not be expected to have effects in the acute timeframe of these studies.

(26) A manuscript detailing the development and phenotyping of these mice is in preparation.

(27) Qi, J.; Lang, W.; Geisler, J. G.; Wang, P.; Petrounia, I.; Mai, S.; Smith, C.; Askari, H.; Struble, G. T.; Williams, R.; Bhanot, S.; Monia, B. P.; Bayoumy, S.; Grant, E.; Caldwell, G. W.; Todd, M. J.; Liang, Y.; Gaul, M. D.; Demarest, K. T.; Connelly, M. A.The use of stable isotope-labeled glycerol and oleic acid to differentiate the hepatic functions of DGAT1 and -2. *J. Lipid Res*. **2012**, *53*, 1106–1116.

(28) Smith, R.; Campbell, A.-M.; Coish, P.; Dai, M.; Jenkins, S.; Lowe, D.; O'Connor, S.; Su, N.; Wang, G.; Zhang, M.; Zhu, L. Preparation and use of arylalkyl acid derivatives for the treatment of obesity. US 20040224997, 2004.